

Investigation of flux dependent sensitivity on single event effect in memory devices

Jie Luo(罗捷), Tie-shan Wang(王铁山), Dong-qing Li(李东青), Tian-qi Liu(刘天奇), Ming-dong Hou(侯明东), You-mei Sun(孙友梅), Jing-lai Duan(段敬来), Hui-jun Yao(姚会军), Kai Xi(习凯), Bing Ye(叶兵), Jie Liu(刘杰)

Citation: Chin. Phys. B . 2018, 27(7): 076101. **doi:** 10.1088/1674-1056/27/7/076101

Journal homepage: http://cpb.iphy.ac.cn; http://iopscience.iop.org/cpb

What follows is a list of articles you may be interested in

Mechanisms of atmospheric neutron-induced single event upsets in nanometric SOI and bulk SRAM devices based on experiment-verified simulation tool

Zhi-Feng Lei(雷志锋), Zhan-Gang Zhang(张战刚), Yun-Fei En(恩云飞), Yun Huang(黄云)

Chin. Phys. B . 2018, 27(6): 066105. **doi:** 10.1088/1674-1056/27/6/066105

Single event effect in a ferroelectric-gate field-effect transistor under heavy-ion irradiation

Yan Shao-An, Tang Ming-Hua, Zhao Wen, Guo Hong-Xia, Zhang Wan-Li, Xu Xin-Yu, Wang Xu-Dong, Ding Hao, Chen Jian-Wei, Li Zheng, Zhou Yi-Chun

Chin. Phys. B . 2014, 23(4): 046104. **doi:** 10.1088/1674-1056/23/4/046104

Large energy-loss straggling of swift heavy ions in ultra-thin active silicon layers

Zhang Zhan-Gang, Liu Jie, Hou Ming-Dong, Sun You-Mei, Zhao Fa-Zhan, Liu Gang, Han Zheng-Sheng, Geng Chao, Liu Jian-De, Xi Kai, Duan Jing-Lai, Yao Hui-Jun, Mo Dan, Luo Jie, Gu Song, Liu Tian-Qi

Chin. Phys. B . 2013, 22(9): 096103. **doi:** 10.1088/1674-1056/22/9/096103

Angular dependence of multiple-bit upset response in static random access memories under heavy ion irradiation

Zhang Zhan-Gang, Liu Jie, Hou Ming-Dong, Sun You-Mei, Su Hong, Duan Jing-Lai, Mo Dan, Yao Hui-Jun, Luo Jie, Gu Song, Geng Chao, Xi Kai

Chin. Phys. B . 2013, 22(8): 086102. **doi:** 10.1088/1674-1056/22/8/086102

Radiation damage effects on power VDMOS devices with composite SiO_2–Si_3N_4 films

Gao Bo, Liu Gang, Wang Li-Xin, Han Zheng-Sheng, Song Li-Mei, Zhang Yan-Fei, Teng Rui, Wu Hai-Zhou

Chin. Phys. B . 2013, 22(3): 036103. **doi:** 10.1088/1674-1056/22/3/036103

Investigation of flux dependent sensitivity on single event effect in memory devices*

Jie Luo(罗捷)[1,2,3], Tie-shan Wang(王铁山)[2], Dong-qing Li(李东青)[1], Tian-qi Liu(刘天奇)[1], Ming-dong Hou(侯明东)[1], You-mei Sun(孙友梅)[1], Jing-lai Duan(段敬来)[1], Hui-jun Yao(姚会军)[1], Kai Xi(习凯)[1], Bing Ye(叶兵)[1], and Jie Liu(刘杰)[1,†]

[1] *Institute of Modern Physics, Chinese Academy of Sciences, Lanzhou* 730000, *China*
[2] *School of Nuclear Science and Technology, Lanzhou University, Lanzhou* 730000, *China*
[3] *University of Chinese Academy of Sciences, Beijing* 100049, *China*

(Received 2 January 2018; revised manuscript received 23 March 2018; published online 25 June 2018)

Heavy-ion flux is an important experimental parameter in the ground based single event tests. The flux impact on a single event effect in different memory devices is analyzed by using GEANT4 and TCAD simulation methods. The transient radial track profile depends not only on the linear energy transfer (LET) of the incident ion, but also on the mass and energy of the ion. For the ions with the energies at the Bragg peaks, the radial charge distribution is wider when the ion LET is larger. The results extracted from the GEANT4 and TCAD simulations, together with detailed analysis of the device structure, are presented to demonstrate phenomena observed in the flux related experiment. The analysis shows that the flux effect conclusions drawn from the experiment are intrinsically connected and all indicate the mechanism that the flux effect stems from multiple ion-induced pulses functioning together and relies exquisitely on the specific response of the device.

Keywords: ion flux, single event effect, GEANT4 simulation, memory device

PACS: 61.82.Fk, 95.75.–z, 24.10.Lx **DOI:** 10.1088/1674-1056/27/7/076101

1. Introduction

Single event effects (SEEs) have become increasingly important as the feature size of the microelectronic devices continue scaling down.[1–3] Tremendous efforts, both experimental and theoretical, have been invested into this field to study the basic mechanism of the effects. Particle flux is an important experimental parameter in ground based irradiation tests. Actually, the natural space is a flux variable environment,[4,5] and the test standards have not specified the particle flux to be used in the ground based experiments.[6–8] In addition, the ion flux during SEE tests is normally much higher than that in real space radiation conditions. Thus, a dedicated study needs to take into account the flux impact on SEEs in microelectronic devices.

In the previous studies, Liu *et al.* introduced "double-hit" to explain the errors in the ADE harden device.[9] Edmonds suggested the flip of triple module redundancy (TMR) harden device is evidently raised at higher flux.[10] Yu *et al.* reported the test result differences between low and high fluxes for various types of devices and found that only certain types of devices exhibit flux dependence.[11] Our research group conducted the flux related experiment using various types of devices covering LET from 10.1 MeV·cm^2/mg to 99.8 MeV·cm^2/mg, and three experimental conclusions were drawn.[12] First, the flux effect is range dependent that memory devices become flux sensitive as the flux increases above 10^3 ions/cm^2·s, i.e., for most cases, the cross section of the single event errors increases. Second, the flux effect is linear energy transfer (LET) dependent that as the LET of the incident ions becomes larger, the flux effect becomes more evident. Third, the flux effect is device dependent so different types of devices show different flux sensitivities.

This paper aims at studying the theoretical mechanism of the flux effect by employing GEANT4 and TCAD simulation methods. Radial charge distributions and the charge collection processes induced by various types of ions used in the ground based experiment are explored. The transient aspect of the heavy-ion track structure in silicon devices, together with the analysis of the specific device response, is investigated to explain the flux impact on SEEs in different memory devices.

2. Simulation method

GEANT4 is a powerful simulation tool kit utilizing the Monte Carlo method to calculate interactions of particles with matter.[13] It is programed in C++ language and widely used in high energy physics, nuclear physics, medical science, space science, etc. In this work, GEANT4 version 10.3 has been used by implementing the newly developed MicroElec model.[14,15] This new model is categorized in low energy electromagnetic physics especially developed for the interactions of particles in silicon by lowering the energy production threshold of secondary electrons down to 16.7 eV, which is

*Project supported by the National Natural Science Foundation of China (Grant Nos. U1532261, 11690041, and 11675233).
†Corresponding author. E-mail: j.liu@impcas.ac.cn
© 2018 Chinese Physical Society and IOP Publishing Ltd

much lower than that in the previous models. With the improvement of the new model, large numbers of discrete secondary electrons can be precisely tracked, giving a much better illustration of the ion track structure.

Three types of ions that are mostly used in the ground based experiments are chosen for the simulation: ^{209}Bi, ^{129}Xe, and ^{86}Kr. In order to get sufficient statistics, the radial charge distribution for each type of ion is calculated by averaging the tracks of 10^6 incident ions.

The geometry used to simulate the radial charge distributions is illustrated in Fig. 1. As reported in Ref. [16], the 90 nm technology featuring a 50 nm gate length for the 1 μm^2 SRAM cell is considered to build the geometry. The world consists of a box of 20 μm×20 μm×8 μm of natural silicon with an over layer of 5 μm, mimicking the thickness of the materials above the transistors of the SRAM cells. Then there is the active layer of 250 nm representing the layer of the studied transistors. To simulate the radial track structure, the energy deposited in this active layer is calculated and stored in a histogram as a function of the radial distance from the center of the ion path. The deposited energy is converted to the density of electron/hole pairs by dividing the value of 3.6 eV, the average energy needed to create an electron/hole pair in silicon.

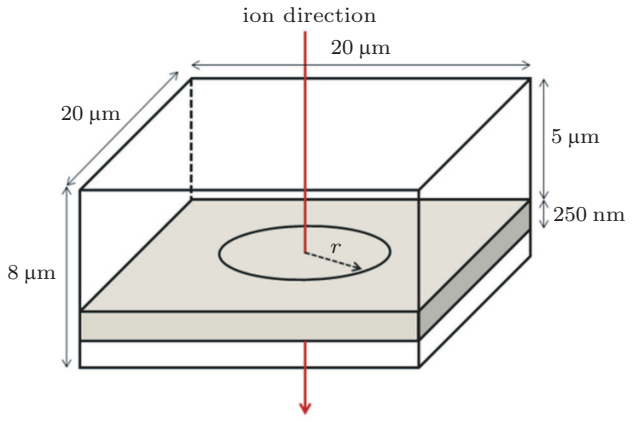


Fig. 1. (color online) The geometry configuration used to simulate radial charge distributions. The active layer is 250 nm thick representing the layer of the studied transistors (not to scale).

The charge collection processes are simulated by the TCAD simulator Synopsys Sentaurus.[17] Figure 2 shows the structure of the NMOS transistor extracted from the SRAM cell reported in Ref. [16]. The gate oxide thickness is 12 nm and the gate length is 50 nm. The color gradation shows the doping concentration for each electrode of the transistor. The ion track structures obtained from GEANT4 simulations are used as the input data in the Synopsys Sentaurus device simulator. To study the worst case scenario, the NMOS transistor is biased in the OFF-state, i.e., the drain is biased at 1.2 V while the gate and source both at 0 V. The ion strikes the device at normal incidence in the middle of the drain area. In order to analyze the transistor response, the simulated transient current at the drain electrode is recorded as a function of time after the ion strike.

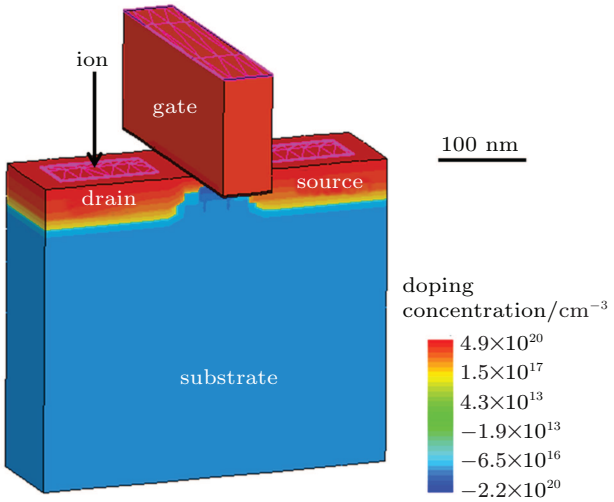


Fig. 2. (color online) Schematic representation of the NMOS transistor with 50 nm gate length. The ion incidents in the middle of the drain area (black arrow).

3. Simulation results

3.1. Radial track profile

The first parameter to check is the LET spectra of the three different ions penetrating into silicon. The LET is calculated using the SRIM software and the LET curves of the three ions are depicted from the incident energy of 1 MeV to 2 GeV (Fig. 3).[18] Each curve shows the same portrait that with the increase of the incident energy, the LET first increases quickly, then the curve reaches the Bragg peak,[19] the largest LET that the ion specie can get. After the Bragg peak, the curve presents a slant plateau that the LET decreases slowly as the ion energy increases. Different ion species have different Bragg peaks; as the ion becomes heavier the Bragg peak of this ion increases. It can be seen that for the same ion, it can have the same LET with two different energies.

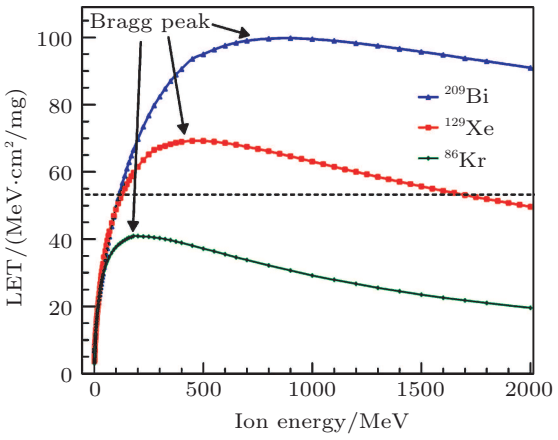


Fig. 3. (color online) LET curve as a function of energy for three different ions. The dotted line shows ^{129}Xe ion at the LET of 53.7 MeV· cm^2/mg with different energies of 130 MeV and 1677 MeV.

To investigate the track structure for the ion that has the same LET but different energy, the simulation is conducted using ^{129}Xe ion at the LET of 53.7 MeV·cm^2/mg with the energies of 130 MeV and 1677 MeV (Fig. 3). The simulation is set to calculate the interactions of a single ion hit, and all the trajectories of the ejected electrons are saved for later visualization. Figure 4 presents a three-dimensional (3D) image of the simulation result. The interaction of ^{129}Xe ion with silicon can produce secondary electrons, the so called δ-rays. These δ-rays can release more electrons, making the interaction process into a cascade. The new model can exhibit the long range δ-rays as well as the low range electrons whose energies fall below 16.7 eV.

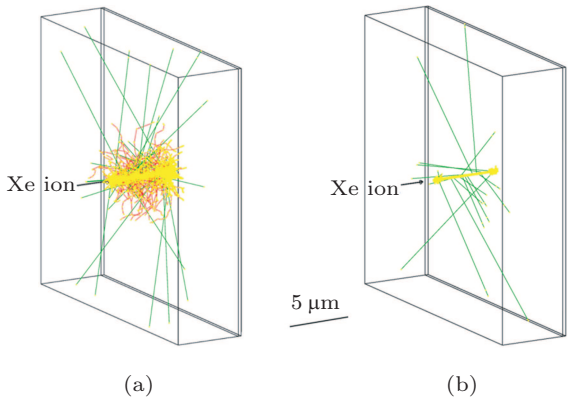


Fig. 4. (color online) 3D visualization of the GEANT4 simulation for ^{129}Xe ion at the LET of 53.7 MeV·cm^2/mg with two different energies: (a) 1677 MeV and (b) 130 MeV.

These two types of ions have the same LET at the surface of silicon that the energy deposition per depth is the same, but the radial profiles of the excited electrons are quite different. The average energy of secondary electrons for the 1677 MeV ^{129}Xe ion is larger than that for the 130 MeV ^{129}Xe ion. Hence, the energetic electrons excited by the 1677 MeV ^{129}Xe ion can penetrate further away from the ion path and deposit their energies in larger distances. On the contrary, the average energy of secondary electrons excited by 130 MeV ^{129}Xe is much lower, and the energy is deposited locally around the track core region.

The ions with the same LET but different energies produce remarkably different radial track structures in silicon. Figure 5 shows the charge density as a function of the radial distance from the ion path of ^{129}Xe ion with the energies of 130 MeV, 1677 MeV, and 550 MeV, the energy at Bragg peak. 130 MeV ^{129}Xe produces a larger charge density than 1677 MeV ^{129}Xe in the volume near the ion path, while further from the ion path ($>$ 10 nm), 1677 MeV ^{129}Xe deposits more charge due to the longer range of δ-rays generated in the interactions.

The radial charge difference results from the energy distribution difference of the δ-rays ejected by the incident ion. The simulation result of the radial charge distributions can be extrapolated to other ions with the same LET but different energies. On the right side of the Bragg peaks in Fig. 2, for the ions with the same LET but different masses and energies, when the ion mass becomes larger, the required incident energy for the ion also becomes larger. Thus, the mean energy of the δ-rays becomes larger, making the charge distribution wider. On the left side of the Bragg peaks, as the ion energy becomes smaller, the mean energy of the δ-rays becomes smaller, making the charge density near the track core region larger.

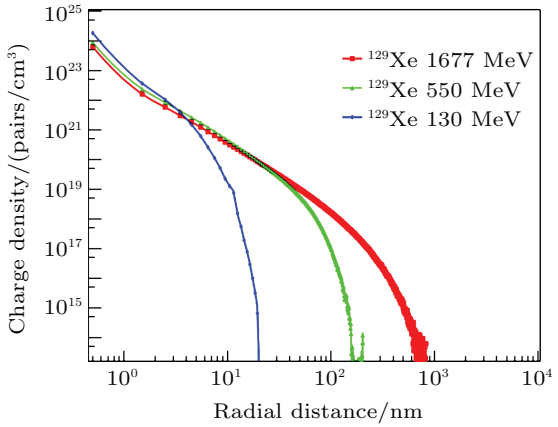


Fig. 5. (color online) GEANT4 simulations of the radial pair density generated by 1677 MeV, 550 MeV, and 130 MeV ^{129}Xe ions. The LET for each ion is 53.7 MeV·cm^2/mg, 69.1 MeV·cm^2/mg, and 53.7 MeV·cm^2/mg, respectively.

The incident energy of the ion plays an important role in determining the track radial profile. To compare the radial charge profiles of different ion spices at the energy of Bragg peaks, ^{209}Bi, ^{129}Xe, and ^{86}Kr are simulated at the energies of 1020 MeV, 550 MeV, and 240 MeV, and the LETs are 99.8 MeV·cm^2/mg, 69.1 MeV·cm^2/mg, and 40.7 MeV·cm^2/mg, respectively. Figure 6 reports the simulation result. As the ion mass increases, the LET at the Bragg peak also increases, not only does the charge radial distribution become wider, but also the charge density at a designated radius becomes larger.

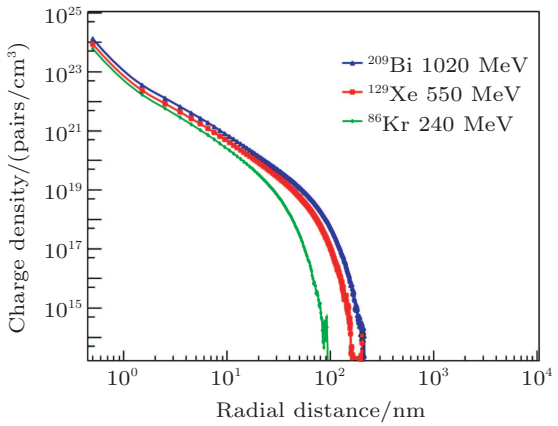


Fig. 6. (color online) GEANT4 simulations of the radial pair density profile generated by 1020 MeV ^{209}Bi ion, 550 MeV ^{129}Xe ions, and 240 MeV ^{86}Kr ion. The corresponding LETs are 99.8 MeV·cm^2/mg, 69.1 MeV·cm^2/mg, and 40.7 MeV·cm^2/mg, respectively.

3.2. Charge collection process

The results concerning the charge collection processes extracted from the Synopsys Sentaurus simulations are reported in Fig. 7, which shows the transient currents as a function of time for the three different ions with the energies at Bragg peaks. Though the general shape of the transient currents is similar, the peak current and transient width are different for different types of ions. The peak current and transient width for the 1020 MeV ^{209}Bi ion with the LET of 99.8 MeV·cm^2/mg are much larger than those for the 550 MeV ^{129}Xe and 240 MeV ^{86}Kr ions, which can be deduced by the fact that the charge distribution is much wider and the charge density is much larger for the 1020 MeV ^{209}Bi ion. It can be seen that the overall charge collection processes for different types of ions may last nano-seconds, yet the exact collection time is dependent on the specific radial charge distribution of the incident ion.

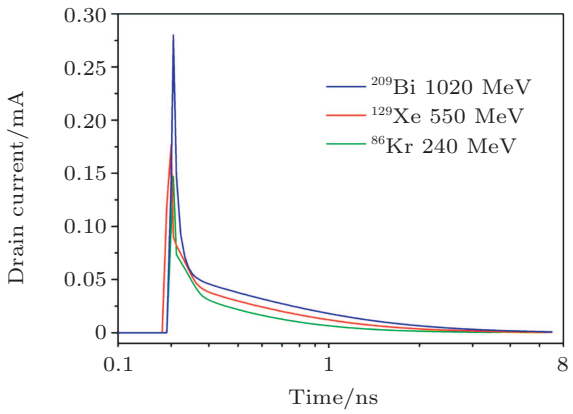


Fig. 7. (color online) Drain current transient in the NMOS transistor as a function of time.

4. Explanations to the flux effect

4.1. Flux range

The experiment results and analysis conclusions from the previous studies indicate that the flux effect might result from two or more ion-induced pulses affecting the storage cell at high flux radiation conditions. Hence, the spatial and temporal aspects of the ion-induced pulses are crucial to the mechanism of the flux related upset process. The results extracted from GEANT4 and TCAD simulations illustrate the charge deposition as well as the charge collection process. The charge collection length may be several micro-meters, and the charge collection time may last for several nano-seconds. If the charge sharing effect is considered,[20] the charge deposited at the strike location may be collected by nearby transistors, making the effective charge collection length even larger and the charge collection time even longer.

Furthermore, the particle incident in the device can cause significant voltage transients propagating in the circuit, affecting the sensitive nodes along the circuitry paths.[21] Thus, the affecting time by a single hit may be prolonged and the affecting area may be extended along the transients' propagating paths in the circuit. Hence, the spatial and temporal requirement for the ion-induced pulses linking together is determined not only by the charge collection process, but more importantly, also by the detailed circuit response of the specific device.

As the flux continues to increase, the global radiation response of the devices will occur, which is termed as the dose-rate effect.[22–24] The transistors in the device are either connected to the power rail or to the ground bus. Each transistor behaves like the collection node under the global irradiation fluence, contributing to the current flow in the power rail or the ground bus. The induced currents across the entire chip can cause a diminished voltage supply, either a drop in V_{dd} and/or a rise in V_{ss}, leading to a reduced noise margin and a lower transient radiation upset threshold. The final states of the cells are randomized by global circuit noises, and thus are more vulnerable to transient perturbations.

The experiment flux threshold of 10^3 ions/cm^2·s marks the boundary below which the flux effect will not happen. This might be explained by the fact that, when the flux is under 10^3 ions/cm^2·s, the opportunity of two ion-induced pulses linking together is relatively low and the dose-rate effect is negligible. The flux effect only occurs at the higher end of the flux range, i.e., when the flux increases above a certain value, the perturbations of multiple pulses coinciding together and the induced global current cannot be ignored. The boundary of 10^3 ions/cm^2·s does not mean that the flux effect will definitely happen when it is above this value, but denotes a strong possibility that the flux effect might happen. For certain type of device, the threshold for the flux effect might be even higher. When the flux continues to increase, there will be more radiation related, various types of internal noises complicating the upset mechanism, i.e., more transient pulses coinciding with other radiation induced noises contribute to the final cause of an SEU. Due to these trends, the error rate in memory parts tends to become higher when subjected to higher flux conditions.

This boundary value is related to the temporal cross sectional distribution of the ion beam, which has something to do with the beam transportation and modulation mechanism of the high energy ion acceleration system. A different accelerator facility may have a different accelerating and transportation mechanism, leading to a different transient cross sectional distribution of the ion beam, and thus a different boundary value for the flux effect.

4.2. LET dependency

As the LET becomes larger, two aspects of the radial charge profile might be changed: the charge distribution radius and the charge deposition density. From the above analysis

about the flux effect, the charge collection length in the device and the charge collection amount by the sensitive node can both contribute to the flux effect, yet in quite different ways. As the charge collection length becomes larger, the chance of direct special connection becomes larger, making the storage cell more likely to be impacted by two or more ions. As the deposited charge density becomes larger, the collected charge by the sensitive node becomes larger, making the disturbing pulse larger and the dose rate effect more significant.

The experiment conclusion is drawn based on the data taken at LETs near the Bragg peaks. Figure 7 shows that for the ions at energies of the Bragg peaks, the larger the LET, the larger the amount of charge collection, and the larger the charge collection area. With the collected charge increased and collection length expanded, the number of provoked transients increases and the dose-rate effect also increases, therefore the chance of the multiple ion-induced pulses linking together increases and the device becomes more sensitive to perturbations. Consequently, the flux effect becomes more evident.

The simulation result suggests that for the ions at the same LET, the radial track profiles are different when the ion masses and energies are different. The charge distribution radius is larger when the ion energy is larger, and the charge density near the track core region is larger when the ion energy is smaller. Hence, the flux effect is not only related to the LET of the incident ion, but also to the ion mass and energy. The question regarding which aspect is more important to the flux effect needs further experiments to verify.

4.3. Device structure dependency

In our previous study, hardened and unhardened devices were subjected to the flux related irradiation experiment. The hardened devices include SOI SRAMs hardened by ADE, bulk-Si flip-flops hardened by dual interlocked storage cell (DICE), and triple modular redundancy (TMR). The test result is consistent with the others that the hardened devices are more flux sensitive than the unhardened ones. As the flux increases, the error rates of the hardened devices are evidently raised.

The most sensitive strike location in the SRAM cell for most technologies is the off n-channeled transistor and off p-channeled transistor.[25] Figure 8 shows the schematic of an SRAM cell hardened by a resistor as an active delay element. If one ion hits the drain of the off n-channeled transistor, the collected current can pull down the struck node potential, initiating the upset process. However, the inserted resistor in the feedback loop can delay the pulse transferring to the off p-channeled transistor, making the SRAM cell hardened to one sensitive node strike. As the ion flux increases, the noise margin might be reduced and there might be an ion-induced pulse affecting the off n-channeled transistor coinciding with another ion-induced pulse affecting the off p-channeled transistor, making the inserted delay element invalid and resulting in a flip of the cell.

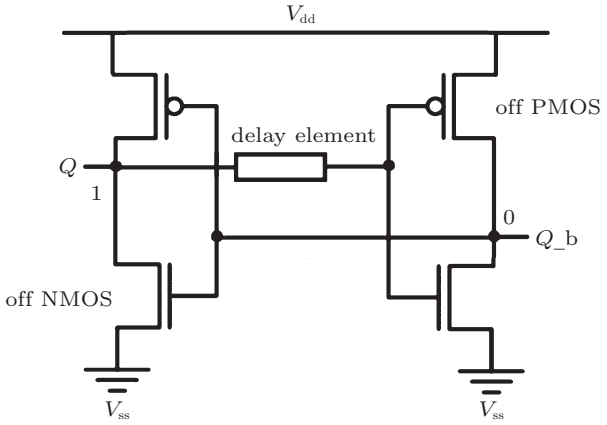


Fig. 8. Schematic of the ADE hardened SRAM cell.

Figure 9 shows the DICE cell which is implemented with storage redundancy to increase the SEU hardness. Without loss of generality, the initial state assumed in the figure is that Q is 0 and Q_b is 1. The logical information is stored in four separated inverters. If one ion hits the off n-channel transistor of inverter B, the information state is unchanged by the coupling effect of the other three redundant inverters and an upset is prevented in the whole storage cell. However, when a second ion hits the off n-channel transistor of inverter D, which is just like writing 0 to the Q_b end, therefore it can cause a wrong memory state and make the whole cell flip.

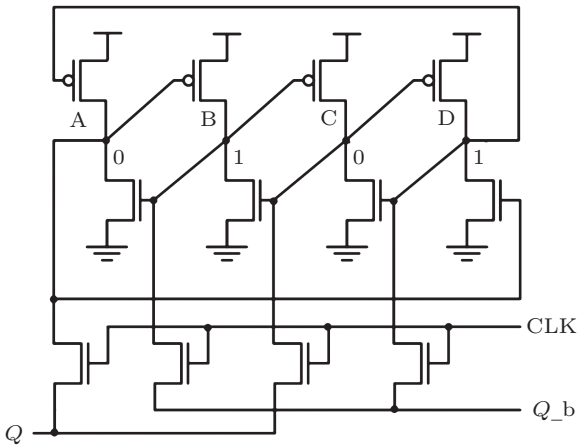


Fig. 9. Schematic of the DICE storage cell.

Figure 10 shows the layout of a TMR circuit with one voter. TMR circuits can mask faults by majority voting and thus can prevent a single fault in the modules that feed the voter inputs. If one module is upset and the other two are unaffected, the output information of the voter is unchanged. If two out of three are upset, the voter inputs receive faulty information and the circuit will produce the wrong output, making the TMR design fail.

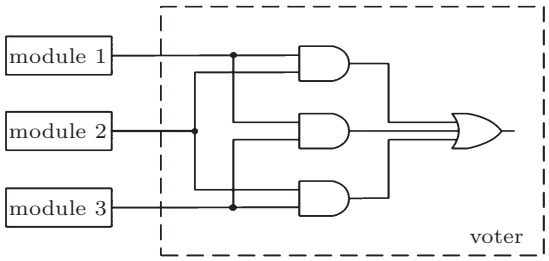


Fig. 10. TMR circuit with one voter.

Single particle hitting a single sensitive node is not likely to cause an upset in the hardened cell. Redundant nodes restore the state of this affected node and prevent an upset in the storage cell. However, as the flux increases above 10^3 ions/cm^2·s, the noise margin might be reduced and there might be two or more ion-induced pulses affecting separated sensitive nodes during the same operation cycle of the storage cell. With multiple ion-induced pulses disturbing the separated sensitive region, it may result in the flip of the hardened cells.

The flux effect is also evidenced from the failure mode of the unhardened bulk-Si SRAM. As the flux increases, the overall cross section of the unhardened SRAM deviates with no specific trend, but the MBUs of more than 3 bits increase as the ion flux increases.[26,27] At the flux higher than 10^3 ions/cm^2·s, four or even higher bits errors appear that must result from more than one ion hitting the adjacent region during the same time interval.

The SEU cross section is denoted by

$$\sigma_{\mathrm{SEU}} = \frac{N_{\mathrm{e}}}{F \cdot N_{\mathrm{b}}}, \tag{1}$$

where N_{e} is the total number of errors, N_{b} is the memory size of the tested device counted by bit, and F is the ion fluence. For the unhardened devices, as the flux increases above 10^3 ions/cm^2·s, besides the single ion induced event, there might be the flux effect related event, which is induced by more than one ion. On one hand, N_{e} tends to increase due to the flux related event, which is the numerator of Eq. (1). On the other hand, the flux related event needs more than one ion, which is counted as ion fluence F in the denominator. These are two completing values in Eq. (1) as the flux increases, so the total σ_{SEU} for the unhardened device deviates with no specific trend. For the hardened device, there is hardly any error at low flux. As the flux increases, the hardened structures are severely disturbed by the ion-induced pulses and the error rate is evidently raised. The increase of total errors N_{e} surpasses the increase of ion fluence F, so the σ_{SEU} becomes larger.

5. Conclusion

GEANT4 and TCAD simulations are performed to analyze the radial charge profile and charge collection time for three different ions mostly used in the ground based experiment. The radial track structure is determined not only by the LET, but also by the mass and energy of the incident ion. The overall charge collection time for different types of ions may last for nano-seconds. The simulation results are analyzed to explain the flux effect, that only at the higher end of the range, higher than 10^3 ions/cm^2·s, can the flux effect occur. The flux effect is related to the amount of collected charge and the size of collection area, therefore the LET and the energy of the incident ion. Different device types are investigated to explain the different flux effect and the reason for the SEE cross section increment is analyzed.

The flux of 10^3 ions/(cm^2·s) is recommended for the ground-based test. As the flux continues to increase, the global radiation response related to the flux effect will occur, making all hardening methods fail. For the flux increases above 10^5 ions/(cm^2·s), the flux effect will be even worse and flux related other perturbations will happen, which is highly unlikely in the real space irradiation condition. However, it provides a method to test whether the device has hardened enough.

The analysis of the mechanism involving the flux effect has a significant impact on designing radiation-hardened circuits at the smaller technology scales. The suggestion is consistent with the test standards that the flux higher than the 10^5 ions/cm^2·s is not recommended. It will play an important role in the selection of test conditions to limit the necessary testing time.

References

[1] Petersen E L, Koga R, Shoga M A, Pickel J C and Price W E 2013 *IEEE Trans. Nucl. Sci.* **60** 1824
[2] Dodd P E, Shaneyfelt M R, Schwank J R and Felix J A 2010 *IEEE Trans. Nucl. Sci.* **57** 1747
[3] Geng C, Xi K, Liu T Q, Gu S and Liu J 2014 *Chin. Phys. B* **23** 086104
[4] Bourdarie S and Xapsos M 2008 *IEEE Trans. Nucl. Sci.* **55** 1810
[5] Barth J L, Dyer C S and Stassinopoulos E G 2003 *IEEE Trans. Nucl. Sci.* **50** 466
[6] *Standard Guide for the Measurement of Single Event Phenomena (SEP) Induced by Heavy Ion Irradiation of Semiconductor Devices*, ASTM F1192, 2000
[7] *Single Event effects Test Method and Guidelines, ESA/SCC Basic Specification* No. 25100, 2002
[8] *Test Procedures for the Measurement of Single-Event Effects in Semiconductor Devices from Heavy Ion Irradiation*, EIA/JESD57, 1996
[9] Liu S T, Nelson D K, Tsang J C, Golke K, Fechner P, HeikkilaW, Brewster N, Cleave R V, Liu H Y, McMarr P J, Hughes H L and Ziegler J F 2007 *IEEE Trans. Nucl. Sci.* **54** 2480
[10] Edmonds L D 2009 *Analysis of Single-Event Upset Rates in Triple-Modular Redundancy Devices*, JPL Publication, 09-6
[11] Yu Q K, Luo L, Zhu M, Sun Y and Tang M 2013 *Proceedings of the 14th European Conference on Radiation and Its Effects on Components and Systems,* September 23–27, 2013, Oxford, UK, p. PJ-5
[12] Luo J, Liu J, Sun Y M, Hou M D, Xi K, Liu T Q, Wang B and Ye B 2017 *Nucl. Instrum. Method Phys. Res. B* **406** 431
[13] Agostinelli S, Allison J, Amako K, *et al.* 2003 *Nucl. Instrum. Method Phys. Res. A* **506** 250
[14] Valentin A, Raine M, Sauvestre J E, Gaillardin M and Paillet P 2012 *Nucl. Instrum. Method Phys. Res. B* **288** 66
[15] Valentin A, Raine M, Gaillardin M and Paillet P 2012 *Nucl. Instrum. Method Phys. Res. B* **287** 124
[16] Thompson S, Anand N, Armstrong M, *et al.* 2002 *International Electron Devices Meeting*, December 8–11, 2002, San Francisco, United Sates of America, p. 61

[17] https://www.synopsys.com/silicon/tcad/device-simulation/sentaurus-device.html
[18] Ziegler J F, Ziegler M D and Biersack J P 2010 *Nucl. Instrum. Methods B* **268** 1818
[19] Liu Z, Chen S M, Liang B, Liu B W and Zhao Z Y 2011 *Sci. China-Phys. Mech. Astron.* **54** 268
[20] Olson B D, Ball D R, Warren K M, Massengill LW, Haddad N F, Doyle S E and McMorrow D 2005 *IEEE Trans. Nucl. Sci.* **52** 2132
[21] Dodd P E, Shaneyfelt M R, Felix J A and Schwank J R 2004 *IEEE Trans. Nucl. Sci.* **51** 3278
[22] Massengill L W and Diehl-Nagle S E 1984 *IEEE Trans. Nucl. Sci.* **31** 1337
[23] Massengill L W and Diehl-Nagle S E 1986 *IEEE Trans. Nucl. Sci.* **33** 1541
[24] Chumakov A I 2006 *Russ. Microelectron.* **35** 156
[25] Dodd P E and Massengill L W 2003 *IEEE Trans. Nucl. Sci* **50** 583
[26] Geng C, Liu J, Xi K, Zhang Z G, Gu S, Hou M D, Sun Y M, Duan J L, Yao H J and Mo D 2013 *Chin. Phys. B* **22** 059501
[27] Geng C, Liu J, Xi K, Zhang Z G, Gu S and Liu T Q 2013 *Chin. Phys. B* **22** 109501